Asian Journal of Chemistry; Vol. 25, No. 6 (2013), 3179-3186

ASIAN JOURNAL OF CHEMISTRY

http://dx.doi.org/10.14233/ajchem.2013.13586

Experimental Research and Numerical Simulation of Coal Char-Catalyzed CO_2 Reforming of CH_4

HAIZHU CHENG[1,*], YONGFA ZHANG[1,*], GUOJIE ZHANG[1] and SUFANG SONG[2]

[1]Key Laboratory of Coal Science and Technology, Ministry of Education and Shanxi Province, Taiyuan University of Technology, Taiyuan 030024, P.R. China
[2]Institute of Chemical and Biological Technology, Taiyuan University of Science and Technology, Taiyuan 030021, P.R. China

*Corresponding authors: Tel: +86 13099071054; E-mail: haoyuxianm@163.com

(*Received*: 13 February 2012; *Accepted*: 14 December 2012) AJC-12544

Experimental research and numerical simulation of coal char-catalyzed CO_2 reformation of CH_4 were done using a small single-hole nozzle reactor. Coal char is known to possess catalytic functions for CH_4-CO_2 reformation. The computational fluid dynamics software was used to simulate a small-scale reactor for the analysis of temperature distribution, flow field and synthetic gas composition. Simulation results show that the reforming reactor demonstrated good flow field and temperature distribution. The CH_4-CO_2 reforming areas had higher temperatures that were deemed suitable for the process. The flow field distribution in the reactor showed that O_2, CO_2 and coke oven gas can be mixed thoroughly to achieve the reaction. The reaction mechanism is a coupling of combustion and reforming reactions at an optimized wall temperature of 1100 K. The H_2/CO ratio was about 1.4-3.0 in the synthesis gas, which is the raw material for methanol synthesis.

Key Words: Coal char catalyst, Numerical simulation, Reforming, Synthetic gas, Flow field, Coke oven gas.

INTRODUCTION

Methane (CH_4) reforming is the process of using carbon dioxide (CO_2) to transform CH_4 into synthesis gas, which can be used to produce liquid fuel, ammonia, methanol, *etc*. It is an important method for methane utilization and is referred to as the gas technology of liquefaction[1]. Conversion of CH_4 and CO_2 into synthesis gas can effectively reduce greenhouse gas emissions and meet the demands of many synthesis processes in the chemical industry. High contents of CH_4 in coke oven gas (COG) and high contents of CO_2 in gasified coal gas can produce synthesis gas through reforming, which have several potential applications, such as in dual gas-head multi-combined technology[2]. Many types of catalyst (*e.g.*, Ni-based, precious metal-based and coal char catalysts) has been tested on CH_4-CO_2 reforming reactors with fixed and fluidized beds at a temperature range of 1073-1573 K. Although a precious metal-based catalyst has better activation, selectivity[3,4] and a lower capacity for carbon deposition resistance than Ni-based and coal char catalysts, its industrial application is restricted due to higher cost[5-7]. Therefore, new and appropriate catalysts that have lower costs are still being investigated. One promising candidate is coal char. Research has shown that coal char can catalyze CH_4-CO_2 reforming[1,8]. Fucheng, *et al.*[9-11] have studied non-catalyzed partial oxidation in natural gas and discovered that there were three main zones in the oven, with the main reaction varying according to the zone. Moreover, the maximum amount of the synthesis gas output and the optimal proportion of oxygen (O_2) and natural gas were subject to the model of the oven used. Currently, no simulation research has yet been reported for coal char as a catalyst in the CH_4-CO_2 reforming reaction. Based on a small experimental device, this study analyzed the preparation, activity and life of the coal char catalyst as well as the impact of the ratio of oxygen flow to coke oven gas on the CH_4 conversion rate and compositions of the main products. The reaction mechanism of a small reforming reactor containing a coal char catalyst was also discussed through numerical simulation, where the temperature distribution, flow field and synthesis gas composition were analyzed. We determined the reaction temperature in the coal char-catalyst zone and the optimized wall surface temperature in the reaction area, providing reference data for future pilot-test experiments.

EXPERIMENTAL

Fig. 1 illustrates the conversion flow chart for the catalyzed partial oxidation in coke oven gas. The conversion reactor mainly consisted of the nozzle and reaction oven.

The main equipment was a 700 mm × 70 mm single-hole nozzle quartz-tube reactor (Fig. 7). Pure oxygen supplied from the oxygen cylinder was injected into the reactor together with

TABLE-1
COMPOSITION, SPECIFIC SURFACE AREA (SSA) AND PORE SPECIFIC VOLUME (PSV) OF THE CATALYST

Ultimate analysis (%, ad)					Ash (%, ad)	SSA (m^2/g)	PSV (cm^3/g)	Modified
C	H	O	N	S				
88.01	1.38	2.45	0.84	0.50	6.87	83.11	0.06	Yes

TABLE-2
COMPOSITION OF COKE OVEN GAS AND LOW HEAT VALUE

	CH_4	H_2	CO	CO_2	N_2	O_2	CmHn	LHV (MJ/Nm^3)
Content (%)	24-28	54-59	5.5-7	3-5	1-3	0.3-0.7	2-3	17

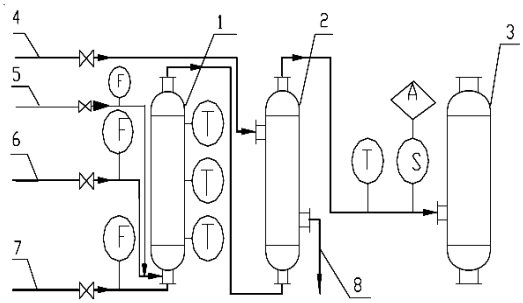

F-Flow, T-Temperature, A-Analyzing, S-Sampling; 1-Reactor, 2-Cooler, 3- Reservoir for Product Gas, 4-Cooling water inlet, 5-CO_2 Inlet, 6- Coke oven gas inlet, 7-O_2 Inlet, 8-Cooling water outlet

Fig. 1. Conversion flow chart for the catalyzed partial oxidation in coke oven gas

the coke oven gas for conversion and were regulated using a ZLB-15 gas glass rotor flow meter. The oxygen, nitrogen, methane, carbon monoxide, carbon dioxide, ethene and ethane contents of the synthesis gas was measured with a GC-950 chromatographic instrument (partial pressure: 0.2 Mpa; column temperature:313.15 K; bridge stream: 60 mA; 13x molecular sieve* 1 m), while the hydrogen content was determined using a GC9890A chromatographic instrument (Partial pressure: 0.4 Mpa; column temperature: 353.15 K; bridge stream: 60 mA; 13x molecular sieve* 1 m). The data were evaluated by a subtraction method. Three temperature measuring points were provided at 23 cm (bottom), 36 cm (middle) and 59 cm (top) from the nozzle. The reaction zone wall temperature was measured by the ST80 infrared thermometer. A platinum-rhodium thermocouple was used to measure the temperature in the reactor. Sampling was also conducted from the synthesis gas outlet, before it was delivered to the chromatograph for analysis. The reactor was water-cooled after the experiments. The outer quartz tube was coated with a nano-adiabatic material (thermal conductivity = 0.025 W/mk) and the coal char catalyst was placed in the middle of the quartz tube reactor (3 kg). The coal char catalyst was prepared through pyrolysis of coal at 1423 K for 1.5 h and crushing the catalyst mass to 30-60 mesh-sized particles. The catalyst was prepared using the impregnation method in a sodium hydroxide solution at room temperature for 3 h. The catalyst was dried in an oven for 12 h at 373 K. Oxygen-bearing functional groups were detected on the surface of the catalyst through X-ray photoelectron spectroscopy. The composition of the catalyst is provided in Table-1, while the composition of the coke oven gas is shown in Table-2.

Analysis of the reaction process: The main chemical reactions that occurred during the catalyzed partial oxidation of the coke oven gas are represented by the following equations:

$$H_2 + 0.5O_2 = H_2O;\ \Delta H^0_{298K} = -241.84\ kJ\ mol^{-1} \quad (1)$$

$$CH_4 + 0.5O_2 = CO + 2H_2;\ \Delta H^0_{298K} = -27.32\ kJ\ mol^{-1} \quad (2)$$

$$CH_4 + 2O_2 = CO_2 + 2H_2O;\ \Delta H^0_{298K} = -802.60\ kJ\ mol^{-1} \quad (3)$$

$$CO + 0.5O_2 = CO_2;\ \Delta H^0_{298K} = -282.96\ kJ\ mol^{-1} \quad (4)$$

$$CH_4 + H_2O = CO + 3H_2;\ \Delta H^0_{298K} = 206.15\ kJ\ mol^{-1} \quad (5)$$

$$CH_4 + CO_2 = 2CO + 2H_2;\ \Delta H^0_{298K} = 247.27\ kJ\ mol^{-1} \quad (6)$$

$$CO_2 + H_2 = CO + H_2O;\ \Delta H^0_{298K} = 115.98\ kJ\ mol^{-1} \quad (7)$$

$$CH_4 = C + 2H_2;\ \Delta H^0_{298K} = 71.56\ kJ\ mol^{-1} \quad (8)$$

Reactions (1)-(4) represented the combustion reaction of the coke oven gas, which were strong exothermic processes that comprised the primary set of reactions, which occurred rapidly, with the complete reaction finishing within several dozens of milliseconds. Reactions (5)-(7) represented the control procedure of the whole process. These were endothermic reactions collectively called the secondary set of reactions. The oxidation process could be finished within 1-2 s[12,13]. To ensure that the secondary reaction could be completed, the appropriate H/D ratio had to be provided for the hearth.

The conversion reactor can be divided according to the main reactions into an upper local area where strong oxidation occurs and a lower-and-middle area where deoxidization-conversion occurs. The partial combustion of H_2, CH_4 and CO provided sufficient heat for the conversion of CH_4 and C_mH_n. The unconverted methane in the lower and middle areas, where deoxidization-conversion occurs, facilitated the reforming reaction with H_2O and CO_2 under high temperatures, generating synthesis gas, such as H_2 and CO, as well as a small amount of CO_2, N_2 and CH_4.

RESULTS AND DISCUSSION

Reaction activity and life of catalyst (O_2 = 0): The life of the coal char catalyst for CO_2 reforming of CH_4 is shown in Fig. 2. The conversion of CH_4 can be divided into two stages. In the first stage, the initial conversion of CH_4 was about 95.2 %. However, as the reaction time extended, the conversion of CH_4 obviously decreased, reaching its lowest rate (about 38.3 %) at 210 min. At the second stage, the conversion of CH_4 remained nearly constant at about 40 %.

Four oxygen-bearing functional groups were detected on the surface of the catalyst through X-ray photoelectron spectroscopy. These were phenolic hydroxyl, carbonyl, carboxyl and lactone. The content of oxygen-bearing functional groups on the catalyst is shown in Table-3.

Table-3 shows that after CO_2-CH_4 reforming, the content of oxygen-bearing functional groups on the catalyst, particularly phenolic hydroxyl and lactone, rapidly decreased from 28.66 and 2.62 % to 4.2 % and 0.2 %, respectively. Thus,

phenolic hydroxyl and lactone played important roles in CO_2-CH_4 reforming and efficiently promoted the conversion of CH_4. However, after the consumption of the phenolic hydroxyl and lactone, the conversion rate of CH_4 dropped. After the phenolic hydroxyl and lactone were completely consumed, the conversion of methane remained nearly constant. Fig. 2 clearly illustrates that the trend of CO_2 conversion is different from that of CH_4. The conversion of CO_2 slightly decreased during the overall CO_2-CH_4 reforming reactions. This indicates that the coal char catalyst had a high activity for CO_2 during the reforming process and that it had better catalyst stability for CO_2-CH_4 reforming at 200 min. This makes it a promising new catalyst for transforming coke oven gas to synthetic gas.

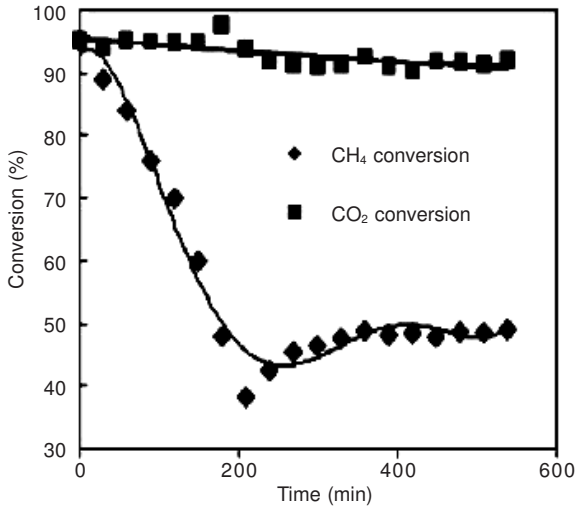

Fig. 2. Life of the coal char catalyst during CO_2-CH_4 reforming (reaction condition: coal char catalyst, temperature = 1223K, CO_2:CH_4 ≈ 1:1, CO_2 flow rate = 120 mL/min, coke oven gas flow rate = 500 mL/min, O_2:0)

TABLE-3
CONTENT OF OXYGEN-BEARING FUNCTIONAL GROUP ON THE CATALYST

Item	Content of oxygen-bearing functional group (%)				
	C–C	Phenolic hydroxyl	Carbonyl	Carboxyl	Lactone
Before reaction	56.60	28.66	6.08	6.04	2.62
After reaction	82.14	4.20	9.79	3.67	0.20

(O_2 > 0): O_2/GAS represented the ratio of oxygen flow to the coke oven gas flow. Table-4 shows some experimental data.

Temperature distribution in the small reactor: Fig. 3 shows the temperature distribution in the reactor when O_2/Gas was increased from 0.18 to 0.40. As the O_2/Gas increased, the bottom temperature rose from 1250-1350 K to 2060-2160 K, the middle temperature rose from 1100-1200 K to 1730-1830 K and the top temperature rose from 1050-1150 K to 1470-1570 K. The temperature gradient observed in the experiment proved that the exothermic reactions occurred before endothermic reactions in the reactor. Measuring by isotope tracer technology, about 25 % CH_4 and total stoichiometric O_2 was found to have been combusted and consumed, respectively, in the catalyst bed inlet[4], which caused the temperature to increase in the reactor. The residual CH_4 reformed into synthetic gas in combination with the H_2O and CO_2 formed in the combustion reaction. The reforming reaction absorbed the heat and caused the temperature to decrease. Since the large H/D ratio and amount of catalyst provided adequate residence time to complete the slower reforming reaction. When the oxygen content in the reactor increased, the gas jet flow became a non-premixed process, which could not be quickly finished during the diffusion process in the oxidation area. While H_2 quickly underwent oxidation, CH_4 and CO still underwent several oxidation reactions, including reactions (1)-(4). Given that some amount of CH_4 was oxidized, the CH_4 content needed to be deoxidized would decrease, thereby reducing heat absorption during the reforming conversion process. This caused the heat of formation due to combustion to increase. Therefore, as O_2/Gas ratio increased, the temperature inside the reactor also increased. As oxygen flow increased along with an equal O_2/Gas ratio, the coke oven gas flow also increased and the total amount of gas which had to undergo partial oxidation reaction also increased. This caused the bottom and middle temperatures in the reactor to rise due to the impact of heat released by the combustion reaction and heat dissipation of the reactor. However, the top temperature was mainly influenced by heat dissipation. The top temperature increases slightly along with an increase in the O_2/Gas ratio. The reaction zone wall temperature was measured at around 1100 K using the ST80 infrared thermometer. Heat dissipation of the reactor was of secondary importance.

Methane and carbon dioxide conversion rate: Fig. 4 shows that the methane conversion rate increased along with O_2/Gas. When the oxygen flow was at 1.4, the O_2/Gas ratio was 0.22-0.26, while the overall CH_4 conversion rate was at 95-97 %. When the CH_4 content was less than 1 %, the reaction reached optimized working conditions. Hence, the CH_4 content in the synthesis gas met the requirements. Isotope tracer technology was used to determine the reaction mechanism of the partial oxidation of CH_4 to synthetic gas in the presence of a catalyst. H_2O and CO_2 existed prior to the generation of H_2

TABLE-4
SOME EXPERIMENTAL DATA (O_2 = 1.2m^3/h, CO_2/CH_4 = 1:1)

O_2/Gas	O_2	N_2	CH_4	CO	CO_2	C_2H_4	C_2H_6	H_2	CO_2 conversion	CH_4 conversion	Temperature (K)		
											23 cm	36 cm	59 cm
0.18	0.29	6.684	4.075	20.85	2.505	1.618	0.037	61.98	0.89	0.694	1250	1200	1150
0.22	0.43	4.75	1.34	21.55	3.32	1.47	0.03	61.37	0.87	0.797	1510	1409	1312
0.26	0.153	2.397	1.09	27.21	6.984	0.743	0.075	59.49	0.89	0.852	1750	1560	1400
0.32	0.225	3.003	0.986	29.27	10.21	0.23	0.014	56.07	0.85	0.950	1980	1730	1500
0.34	0.257	3.388	0.479	30.07	13.39	0.152	0.023	52.26	0.84	0.976	2050	1770	1530
0.38	1.156	7.735	0.105	27.77	18.11	0.039	0.017	45.07	0.82	0.995	2160	1830	1570

and CO and the consumption of H_2O and CO_2 begun while H_2 and CO was being generated. It showed that the reaction is based on a combustion-reforming mechanism[4]. The incombustible CH_4 and CO_2, as well as H_2O, had a reforming reaction, which was an endothermic deoxidation reaction. The heat needed for the reaction was supplied by the exothermic reaction in the oxidation area. As the O_2 flow increased, the temperature inside the reactor also increased. The CH_4 conversion in the presence of coke oven gas [reactions (5) and (6)] were endothermic reactions (Fig. 3). Higher temperatures favoured more CH_4 conversion. The generated CO and H_2 acted as raw materials for the synthesis of methanol and F-T synthesis.

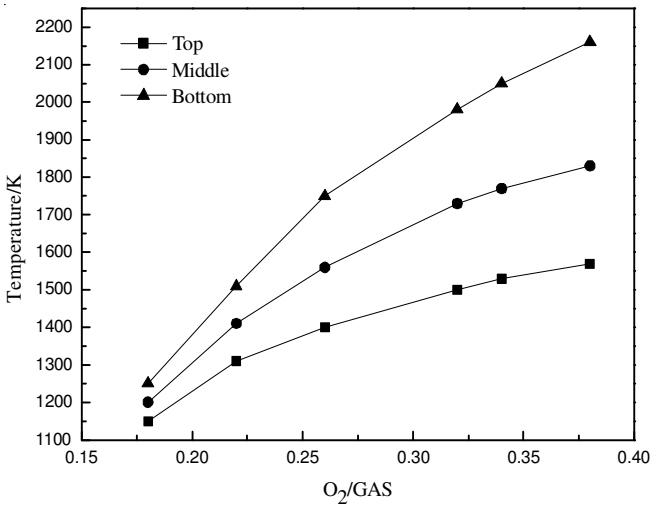

Fig. 3. Influence of O_2/Gas on the reactor temperature (experiment)

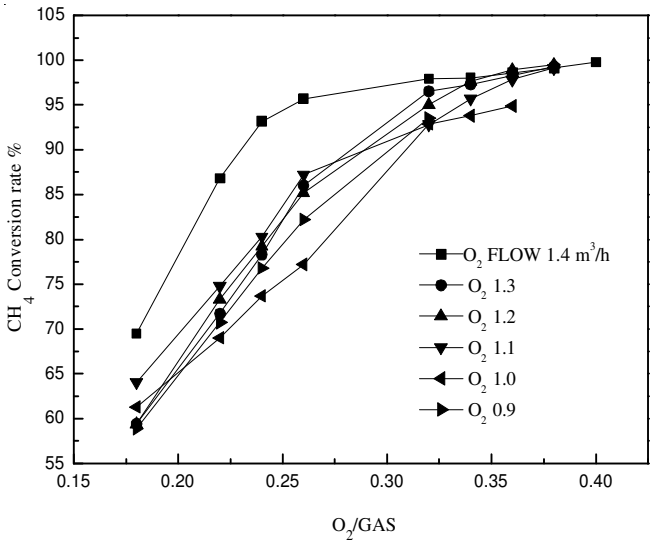

Fig. 4. Dependence of the CH_4 conversion rate on the different levels of O_2/Gas

In this study, CO_2/CH_4 represents the ratio of CO_2 flow to CH_4 flow. Fig. 5 shows that the CO_2 conversion rate decreased when CO_2/CH_4 increased. This could be due to reduced quantity of CO_2 after reforming as a result of the decrease in CH_4 content. This clearly illustrates that the trend of CO_2 conversion is different from that of CH_4. The conversion of CO_2 is mainly due to reaction (6).

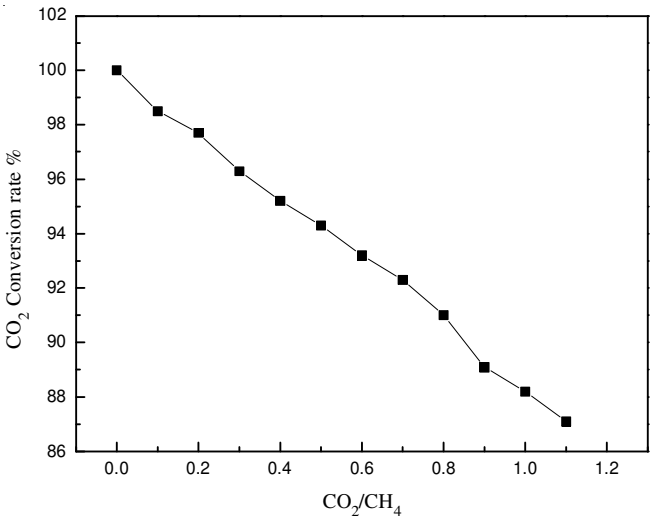

Fig. 5. Dependence of CO_2 conversion rate on CO_2/CH_4

Analysis of H_2/CO ratio in synthetic gas: As shown Fig. 6, the H_2/CO =1.4-3.0 is decreased with increasing O_2 flow. When increasing the O_2/Gas ratio from 0.18 to 0.40, the CO content increased from 20 to 29 % and the H_2 content reduced from 65 to 42 %. The H_2/CO ratio decreased is mainly due to the combustion reaction for H_2 increasing with increasing O_2 flow. Hence, the H_2/CO ratio in synthesis gas can be adjusted by adjusting the O_2/Gas ratio. A theoretically required for synthesize methanol by H_2/CO is about 2.0.

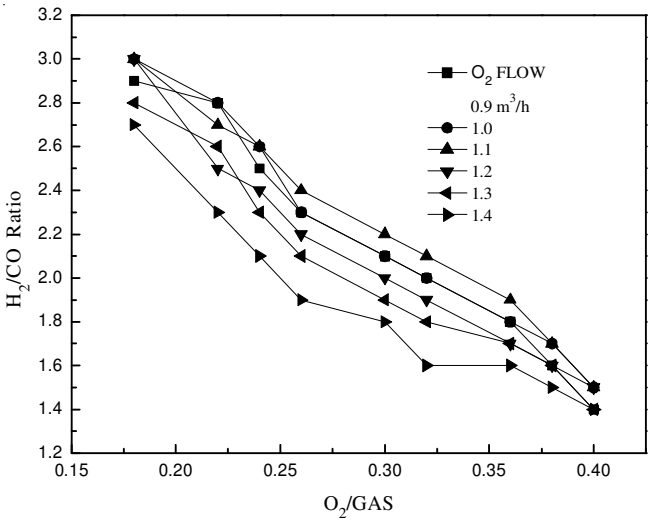

Fig. 6. H_2/CO ratio in the synthetic gas

Numerical simulation of the small reactor

Establishment of the geometric model

Geometric model: The device illustrated in Fig. 7 is a geometric solid with axial symmetry measured in millimeters. Therefore, it can be simplified into a two-dimensional axial-symmetry calculation.

Mathematical formulation: For steady, incompressible flow, the following forms of the mass, momentum, energy and species conservation equations that take into account the effects of turbulence are well-known. However, some considerations were made for the particular case being studied.

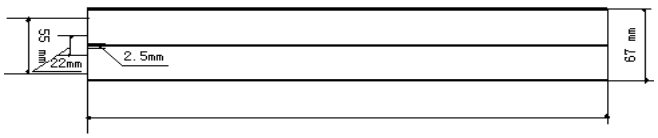

Fig. 7. Geometric model of the small reactor

Momentum equations for porous media in FLUENT: The coal char catalyst is a porous material. Porous media are modeled by adding a momentum source term to the standard fluid flow equations. The source term was composed of two parts, a viscous loss term [Darcy, the first term on the right-hand side of eqn. 9] and an inertial loss term [the second term on the right-hand side of eqn. 9]

$$S_i = -(\sum_{j=1}^{3} D_{ij}\mu_{ij}v_j + \sum_{j=1}^{3} C_{ij}\frac{1}{2}\rho v_j|v_j|) \quad (9)$$

where, S_i is the source term for the *i*th (x, y, or z) momentum equation and D and C are prescribed matrices. This momentum sink contributed to the pressure gradient in the porous cells, creating a pressure drop that was proportional to the fluid velocity (or velocity squared) in the cell. To recover the case of simple homogeneous porous media [eqn.10]:

$$S_i = -(\frac{\mu}{\alpha}v_j + C_2\frac{1}{2}\rho v_i|v_j|) \quad (10)$$

where, α is the permeability and C_2 is the inertial resistance factor, simply specifying D and C as diagonal matrices with $1/\alpha$ and C_2, respectively, on the diagonals (and zero for the other elements).

Treatment of the energy equations in porous media: FLUENT solves the standard energy transport equation [eqn. 11] in regions of the porous media, with modifications to the conduction flux and the transient terms only. In the porous media, the conduction flux used an effective conductivity and the transient terms included the thermal inertia of the solid region on the medium:

$$\frac{\partial}{\partial t}[\gamma\rho_r E_f + (1-\gamma)\rho_s E_s] + \nabla[\vec{v}(\rho_f E_f + \rho)] = \nabla\left[k_{eff}\nabla T - \sum_i h_i J_j + (\bar{\tau}_{eff}\vec{v})\right] + S^h_f \quad (11)$$

where, E_f is the total fluid energy, E_s the total solid medium energy, γ the porosity of the medium, k_{eff} is the effective thermal conductivity of the medium and S^h_f is the fluid enthalpy source term.

Turbulence model: The standard k-ε model equation is the most popular turbulence model applied in hydromechanics simulation. For uncompressed fluids, the standard k-ε model equation is as follows [eq.12, 13 and 14][14]:

$$\frac{\partial(\rho k)}{\partial t} + \frac{\partial(\rho k u_i)}{\partial x_i} = \frac{\partial}{\partial x_j}\left[\left(\mu + \frac{\mu_t}{\sigma_k}\right)\frac{\partial k}{\partial x_j}\right] + G_k - \rho\varepsilon \quad (12)$$

$$\frac{\partial(\rho\varepsilon)}{\partial t} + \frac{\partial(\rho\varepsilon u_i)}{\partial x_i} = \frac{\partial}{\partial x_j}\left[\left(\mu + \frac{\mu_t}{\sigma_\varepsilon}\right)\frac{\partial\varepsilon}{\partial x_j}\right] + \frac{C_{1\varepsilon}\varepsilon}{k}G_k - C_{2\varepsilon}\rho\frac{\varepsilon^2}{k} \quad (13)$$

$$\mu_t = \rho C_\mu \frac{k^2}{\varepsilon} \quad (14)$$

where, the model constants are: $C_{1\varepsilon} = 1.44$, $C_{2\varepsilon} = 1.92$, $C_\mu = 0.09$, $\sigma_k = 1.0$, $\sigma_\varepsilon = 1.3$

P1 radiation model [eqn. 15]

$$\frac{dI(\vec{r},\vec{s})}{ds} + (a+\sigma_s)I(\vec{r},\vec{s}) = an^2\frac{\sigma T^4}{\pi} + \frac{\sigma_s}{4\pi}\int_0^{4\pi} I(\vec{r},\vec{s}')\phi(\vec{r},\vec{s}')d\Omega' \quad (15)$$

where, $\vec{r}$ is the position vector, $\vec{s}$ is the direction vector, $\vec{s}'$ is the scattering direction, s is the stroke length, a is the absorption coefficient, n is the refraction coefficient, σ_s is the scattering coefficient, σ is the Stefan-Boltzmann constant, I is the radiation intensity, T is the local temperature, Φ is the phase function and Ω' is the space solid angle.

Methods of simulation: The model was established using GAMBIT. The calculation regions were divided through a quadrilateral mesh. The small-sized oxygen entrance and the large flow rate combined into a more crucial initial reaction. Therefore, the encrypted grid was adopted in the region near the central axis entrance. There were a total of 50381 grids. Control equations were dispersed using the finite volume method. The high temperature combustion and reaction (HTCR) processes in gas were studied by using the computational fluid dynamics (CFD) software, fluent, which can simulate a two or three-dimensional physical model with the k-ε turbulent viscous model, PDF non-premixed combustion species model and P1 radiation model. The porous medium model was adopted in the analysis of the regions of the coal char catalyst. For the outlet of the main reactor, the pressure was set at 1.0 atm. Assuming a fully developed flow, the turbulent intensity at the inlet and outlet could be estimated with [eqn. 16]:

$$I_{g(L)} = 0.16(Re)^{-1/8} \quad (16)$$

The wall boundary conditions were no-slip boundary conditions. For the evaluation of wall effect on turbulence, the near-wall treatment employed the standard wall functions. There was a heat transfer between the gas and the wall, allowing the energy equation to work. The wall surface temperature changed along the tube. Therefore, using fluent wall surface division technology, the wall surface was divided into 111 sub-areas. On the assumption that the neighboring sub-area temperature difference was 3 K, the wall surface temperature boundary condition was established.

Simulation results and discussion: The simulated parameters were calculated based on the above-mentioned models. Using the CFD software platform, the simulation results were calculated with the following considerations: the external condition of the simulation was the ambient temperature and the border condition was the natural convection heat exchange made between the reactor and air at normal temperature.

Fig. 8 represents the simulation nephogram of the temperature distribution in the reactor. The different colours in the nephogram represented the different temperatures in the reactor. In contrast with the true reactor experimental image (Fig. 9), the simulation flame and experimental flame profiles were similar and the flame lengths were approximately equal. This confirmed that the simulation theory and the model were reasonable.

Fig. 10 illustrates the maximum temperature and outlet temperature simulation results in the reactor (O_2 flow = 1.2 m^3/h, wall surface temperature = 1100 K) when the coke oven

gas flow was changed and the O_2/Gas changed from 0.18 to 0.40. The maximum temperature had a linear distribution and rose slightly from 2926 to 3080 K as the O_2/Gas increased. The approximately equal maximum temperatures were due to the good coupling between the exothermic combustion and the endothermic reforming reactions. As O_2/Gas increased, the various temperatures also rose: outlet temperature (1139 to 1488 K), bottom temperature (1262 to 2144 K), the middle temperature (1211 to 1848 K). The top temperature only slightly increased from 1162 to 1584 K. The simulation results were consistent with the experimental results.

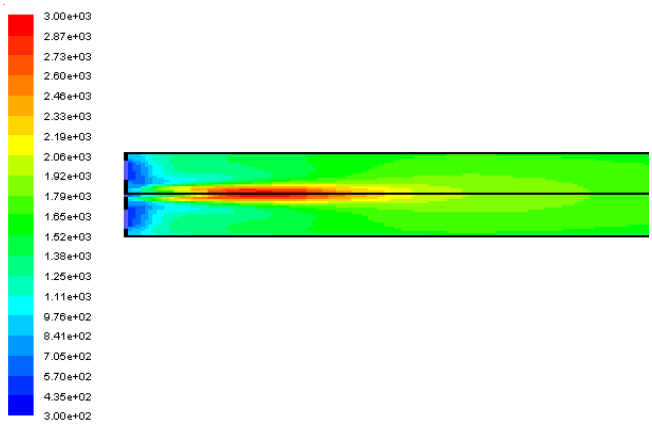

Fig. 8. Temperature distribution map of the single-hole nozzle reactor (simulation)

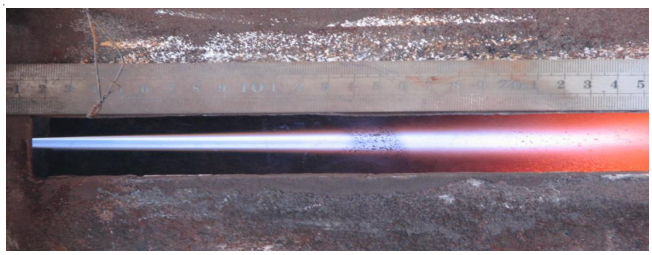

Fig. 9. Experiment flame image

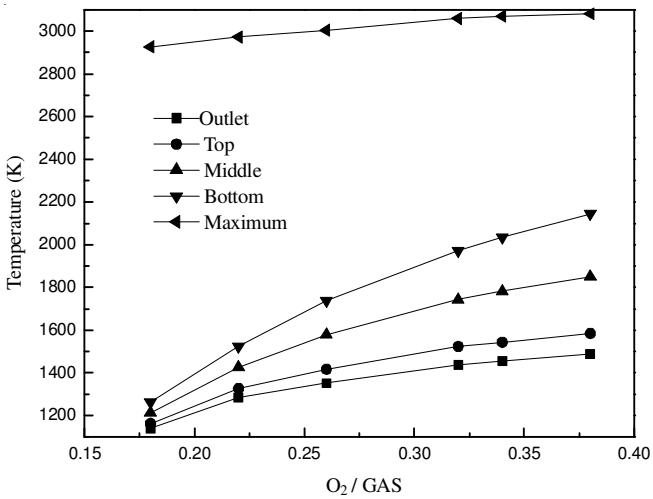

Fig. 10. Influence of O_2/Gas on the reactor temperature (simulation)

Fig. 11 shows the simulation results of the main components in different reaction temperatures. The volume fraction of H_2 decreased from 66.17 to 43.29 %, CO decreased from 23.25 to 20.2 %, CO_2 increased from 1.79 to 6.7 % and CH_4 decreased from 8.705 to 0.105 %. The effective synthetic gas (H_2 + CO) decreased from 89.4 to 63.5 % and H_2/CO decreased from 2.8 to 2.14. The simulated data is in good agreement with the experimental data.

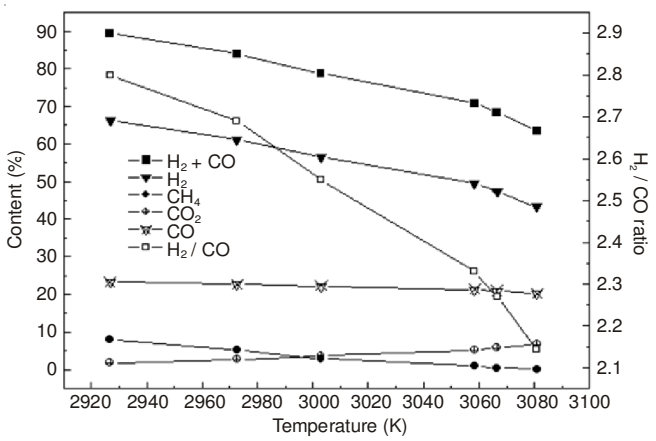

Fig. 11. Contents of the main outlet gas under different reaction temperatures

Fig. 12 is the simulation nephogram of the flow field distribution. The different colours represent the different flow velocities. The flow field was attributed to the turbulent jet. Because the reactor diameter was maintained even without the sudden expansion and contraction of the variable cross-section, no vortex was observed. The combustion reaction occurred mainly close to the entrance and away from the nozzle. It relied on jet turbulent mixing, which was consistent with the laws of hydrodynamics. The coal char catalyst can be placed in the middle of the high temperature area to promote CO_2-CH_4 reforming. The reactor had a big H/D ratio. Therefore, the reactants had a long residence time, guaranteeing that CO_2-CH_4 and H_2O-CH_4 reforming reactions could be completed.

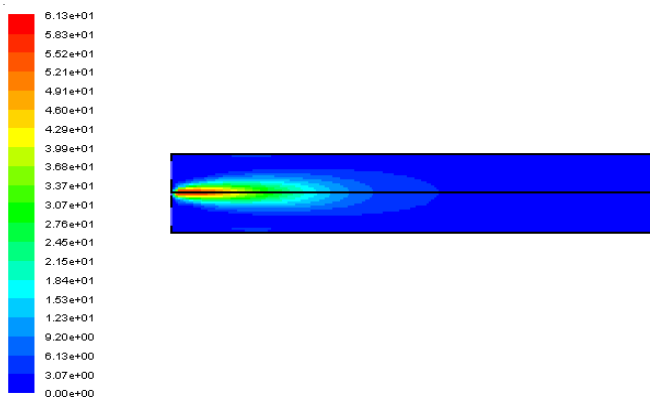

Fig. 12. Flow field distribution map of the single-hole nozzle reactor

Fig. 13 is the simulation map of the axis temperature distribution in the reactor. It showed a rapid rise of the temperature of the system in the initial stage of the reaction and a nearly vertical growth condition. This explained the dramatic increase in the temperature after the coke oven gas and O_2 entered the reactor and the reaction conditions reached the ignition temperature. The temperature distribution indicated

that there was initially an increase in the temperature, representing a mainly exothermic reaction. In other words, H_2, CH_4, C_2H_4 and C_2H_6 had a combustion reaction, which enabled the temperature to increase dramatically to the maximum temperature. These combustion reactions emitted heat, which was advantageous for CH_4 reforming. It enabled the CH_4 reforming reaction to gradually occupy a dominant position. Since the reforming reaction was endothermic, the temperature gradually dropped. The simulation result is consistent with theoretical thermodynamic analysis.

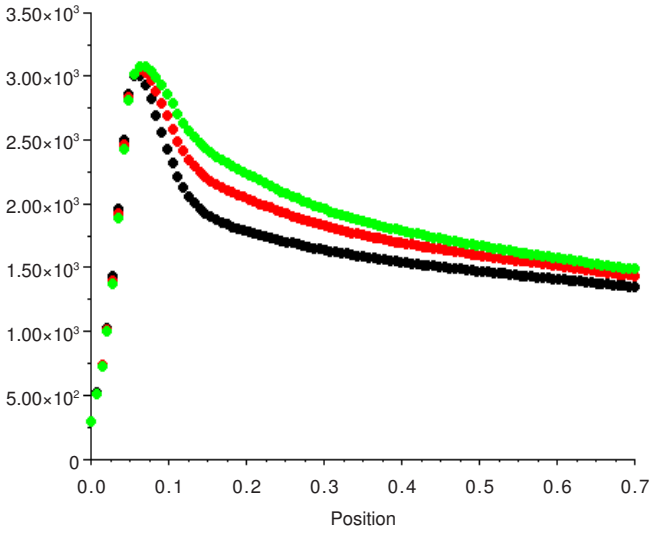

Fig. 13. Axial temperature distribution at different inlet O_2/Gas ratios

Fig. 14 shows the simulated nephogram of H_2 and CO distribution in the reactor (local area was enlarged). The different colours represent different volume contents of the components. Fig. 15 is the axis distribution of the major components. A comparison of a and b was conducted for the H_2 and CO values and the H_2/CO ratio was measured at about 2.5. The CH_4 content also tended towards 0, with a CO_2 content that was lesser than 4 % at the operating condition. According to reaction (17), H_2 and CO can theoretically synthesize methanol by:

$$2H_2 + CO = CH_3OH \quad (17)$$

Reaction (17) shows that theoretical requirements for methanol synthesis are: a H_2/CO ratio of about 2.0. The CH_4 and CO_2 concentrations, as well as the H_2/CO ratio, were control the main parameters. Experimental and simulation results showed that the test system using the coal char-catalyzed CO_2-CH_4 reforming from coke oven gas to generate synthesis gas had reasonable a H_2/CO ratio, CH_4 concentration and CO_2 concentration, thereby making the conversion method feasible.

Comparison between the experimental results and simulations: The simulation results of the single-hole nozzle under 1.2 m^3/h of oxygen and 3.13 m^3/h gas are shown below (Tables 5 and 6).

Tables 5 and 6 shows that the maximum temperature was at 3090 K and the experimental value matched the simulated value very well. This shows that the simulation theories and the models are correct and suitable for this kind of experiment.

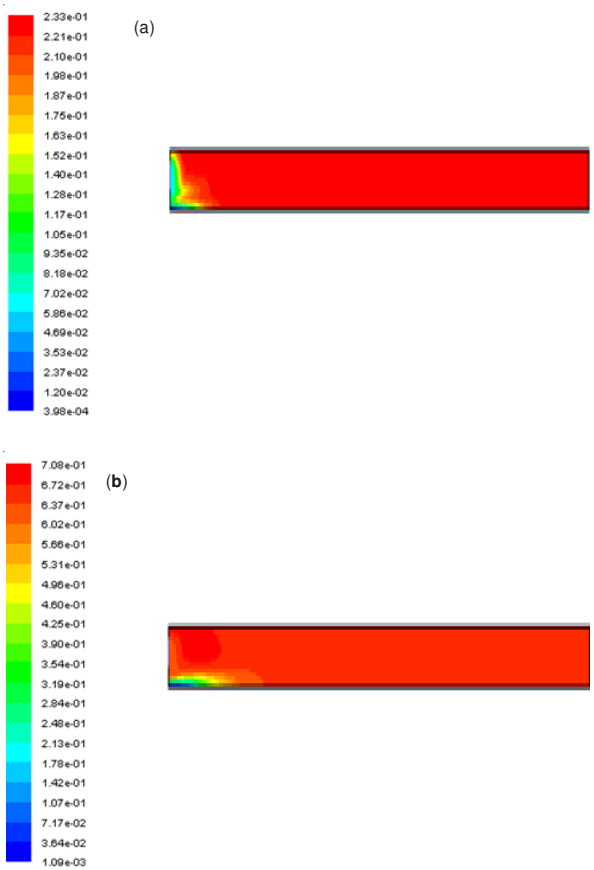

Fig. 14. (a) CO and (b) H_2 distributions inside the reactor

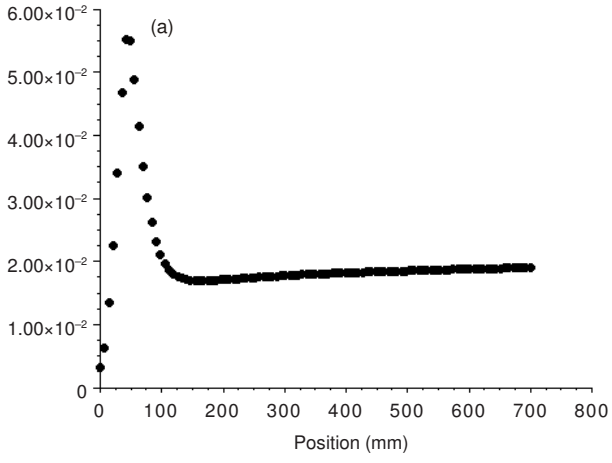

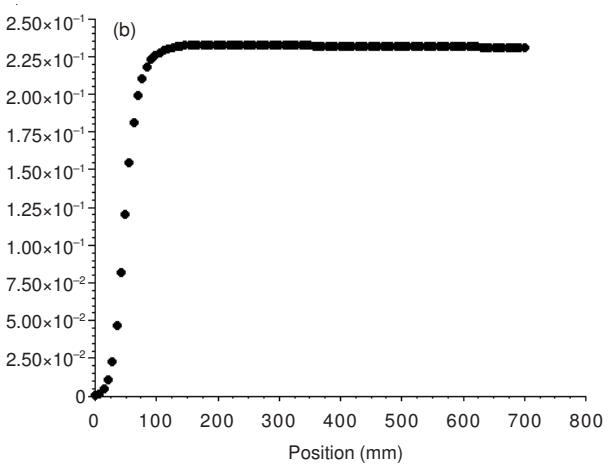

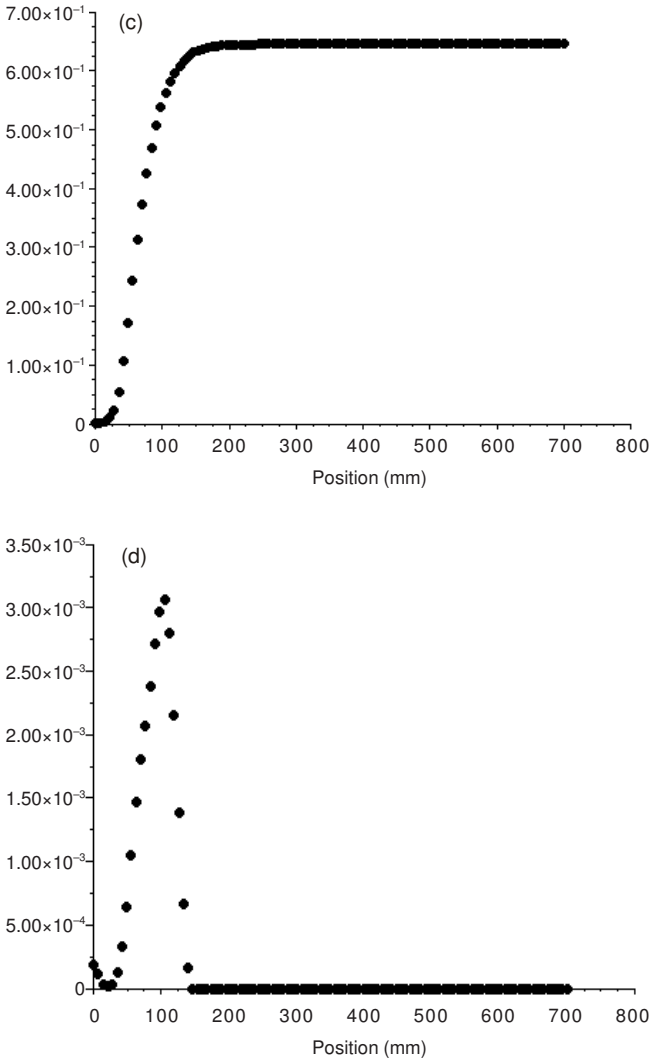

Fig. 15. Axial distribution of the major components: (a) CO_2, (b) CO, (c) H_2 and (d) CH_4

TABLE-5
COMPARISON BETWEEN THE EXPERIMENTAL RESULT AND SIMULATION (TEMPERATURE)

	Temperature (K)		
	Bottom	Middle	Top
Experiment value	1510	1409	1312
Simulated value	1524	1425	1326

TABLE-6
COMPARISON BETWEEN THE EXPERIMENTAL RESULT AND SIMULATION (COMPONENT)

Component (mol %)	H_2	CO	CO_2	CH_4	C_2H_4	C_2H_6	N_2	O_2
Simulation	59.11	22.62	3.37	1.32	1.21	0.99	4.66	2.02
Experiment	61.37	21.55	3.32	1.34	1.47	0.03	4.75	0.43

Conclusion

• Experimental research and simulation results on a small reactor showed that the outlet H_2 gas content was 50-70 % and the CO content was 20 %, giving a H_2/CO ratio of 1.4-3.0 in the synthesis gas. An H_2/CO ratio of about 2.0 was needed to synthesize methanol.

• Temperature simulation on the reforming reactor showed that coal char catalyst exited within a temperature range of 1173-1673 K. However, relevant research has shown that coal char-catalyzed CO_2 reforming of CH_4 started at 873 K and that catalysis was optimal at 1473 K. Therefore, the reforming reactor was designed with an appropriate temperature field. Temperature, flow field and H_2/CO ratio can be adjusted by adjustment O_2/Gas.

• The reaction mechanism inside the reactor was a coupling of combustion and reforming reactions. Reactions 1-6 can simultaneously exist. The position of the maximum temperature point remained unchanged throughout the whole reaction. Approximately constant maximum temperatures can be fully explained with the mechanisms involved.

• The oxygen-bearing functional group exist on the coal char catalyst surface and the oxygen-bearing functional group can accelerate CO_2-CH_4 reforming. The result indicated that the oxygen-bearing functional group (C-O) on the coal char catalyst surface was the active sites of the coal char catalyst The oxygen-bearing functional group (C-O) on the coal char catalyst surface is favourable to the adsorption and dissociation of methane, further, the oxygen-bearing functional group (C-O) on the coal char catalyst surface, active sites, may speed up coke gasification by CO_2.

ACKNOWLEDGEMENTS

This work was supported by the National Basic Research Program of China (2005CB221202), the Innovation Team Funds Scheme and the School Funds of the Taiyuan University of Technology.

REFERENCES

1. G. Zhang, Y. Dong, M. Feng, Y. Zhang, W. Zhao and H. Cao, *Chem. Eng. J.*, **156**, 519 (2010).
2. L. Yang, Y. Dong, Y.F. Zhang and K.C. Xie, *Shanxi Energy Conservation*, **1**, 1 (2006).
3. X. Wu and S. Kawi, *Catal. Today*, **148**, 251 (2009).
4. Q. Wang, Y. Cheng and Y. Jin, *Catal, Today*, **148**, 275 (2009).
5. M. Nagai, K. Nakahira, Y, Ozawa, Y, Namiki and Y, Suzuki, *Chem. Eng. Sci.*, **62**, 4998 (2007).
6. M. Haghighi, Z.-Q. Sun, J.-H. Wu, J. Bromly, H.L. Wee, E. Ng, Y. Wang and D.-K. Zhang, *Proceed. Combust. Inst.*, **31**, 1983 (2007).
7. Q. Jing, H. Lou, J. Fei, Z. Hou and X. Zheng, *Int. J. Hydrogen Energy*, **29**, 1245 (2004).
8. Y.J. Li, W. Zhao and Y.F. Zhang, *Coal Conversion*, **28**, 1 (2005).
9. F.C. Whang and Z.H. Dai, *Coal Chem. Eng.*, **2**, 4 (2006).
10. F.C. Whang and W.F. Li, *Petroleum Chem. Eng.*, **1**, 47 (2006).
11. Z.H. Dai and F.C. Whang, *Chem. Eng.*, **3**, 13 (2005).
12. M. Onozaki and K. Watanabe, T. Hashimoto, H. Saegusa and Y. Katayama, *Fuel*, **85**, 143 (2006).
13. T. Sreethawong, P. Thakonpatthanakun and S. Chavadej, *Int. J. Hydrogen Energy*, **32**, 1067 (2007).
14. F.J. Wang, Analysis on Calculation of Hydromechanics, Tsinghua University Press, Beijing (2004).